# *CHAPTER- VIII*

## *Evidence for Isostructural Phase Transition and Linear Magnetoelectric Coupling in Multiferroic $(Bi_{0.8}\ Pb_{0.2})(Fe_{0.9}Nb_{0.1})O_3$ Solid Solution*

## 8.1 Introduction

There are two promising families of magnetoelectric multiferroics. $TbMnO_3$ [Kimura et al. (2003)], $TbMn_2O_5$ [Hur et al. (2004)], $Ni_3V_2O_8$ [Lawes et al. (2005)] and $MnWO_4$ [Taniguchi et al. (2006)] belong to the first class of compounds in which the development of magnetic spin spiral leads to the appearance of very weak improper ferroelectric polarization ($\sim 10^{-2}$ $\mu C/cm^2$) [Kimura et al. (2003), Cheong and Mostovoy (2007)] but very strong magnetoelectric coupling [Goto et al. (2004)]. However, the Néel temperature for the transition to the multiferroic state in these materials is rather low (e.g. $T_N < 40$ K in $TbMnO_3$) [Cheong and Mostovoy (2007)]. Recently giant improper ferroelectricity with an order of magnitude higher remanent polarization ($P_s \sim 0.28$ $\mu C/cm^2$) and significantly higher $T_N \sim 90$ K has been reported in a new multiferroic compound $CaMn_7O_{12}$ of this family raising the hope for potential application of this class of materials in the near future [Johnson et al. (2012)]. The most promising material in the second class of multiferroics is $BiFeO_3$ which shows a very high proper ferroelectric phase transition temperature with $T_C \sim 1103$ K and magnetic transition $T_N \sim 643$ K [Kaczmarek and Pajak (1975), Roginskaya et al. (1966)]. $BiFeO_3$ also shows extremely large ferroelectric polarization (>100 $\mu C/cm^2$) [Lebeugle et al. (2007A), Lebeugle et al. (2007B)] which is 3 to 4 orders of magnitude higher than that in the first class of compounds.

However, the magnetoelectric coupling is rather weak in $BiFeO_3$ because its complex spiral spin structure does not permit linear magnetoelectric coupling. The

magnetic structure of $BiFeO_3$ basically corresponds to a canted G-type antiferromagnetic ordering which in principle should exhibit weak ferromagnetism and linear magnetoelectric coupling. However, because of the superimposed incommensurate spiral modulation of the spin structure with an approximate periodicity of 62 nm, the net magnetization cancels out over the spin spiral length scale. As a result, $BiFeO_3$ can exhibit only second order magnetoelectric coupling which is much weaker than the linear magnetoelectric coupling [Schmid (1973)].

Many current investigations seek to suppress the spiral spin structure of $BiFeO_3$ in an effort to release the inherent magnetization of the canted G-type antiferromagnetic structure leading to linear magnetoelectric coupling at room temperature [Popov et al. (1993), Sosnowska et al. (2002), Wang et al. (2005), Singh et al. (2008), Singh et al. (2011)] using different strategies. In single crystals of $BiFeO_3$, application of a high magnetic field ($H \geq 20$ Tesla) along [001] has been shown to induce a phase transition from the spatially modulated antiferromagnetic spiral spin structure to a spatially homogeneous antiferromagnetic structure [Popov et al. (1993)]. This transition results in the release of the locked-in magnetization, which is reported to be of the order of 0.3 emu/g at 10 K [Wang et al. (2005)]. Yet another way to destroy the spiral spin structure of $BiFeO_3$ is to use nanocrystalline $BiFeO_3$ having particle sizes smaller than the wavelength (~ 62 nm) of the spiral-modulated spin structure. The $BiFeO_3$ nanoparticles with size less than 62 nm have been reported to exhibit large values of spontaneous magnetization ($M_S$ ~ 1.55 emu/g at 300 K) in comparison with the particles having sizes greater than 62 nm [Park et al. (2007)] because of enhanced contribution from the surface layers as well. The spiral spin structure seems to be

suppressed under epitaxial constraints which are also reported to lead to saturation magnetization values of $M_S$ ~ 0.06 $\mu_B$/Fe [Eerenstein et al. (2005)]. Yet another convenient way of destroying the spiral spin structure is by chemical substitutions leading to weak ferromagnetism and linear magnetoelectric coupling. Doping of $BiFeO_3$ with $La^{3+}$ is known to produce weak ferromagnetism in $Bi_{0.7}La_{0.3}FeO_3$ [Sosnowska et al. (1993)]. In the mixed system $(Bi_{0.8}La_{0.2})(Fe,Ga)O_3$-45% $PbTiO_3$, a remanent magnetization ($M_r$) of ~ 0.15 and 0.3 emu/g at T = 300 K and 5 K, respectively, have also been reported [Wang et al. (2005)]. The fact that the values of $M_r$ (~ 0.3 emu/g) reported at low temperatures in $BiFeO_3$ solid solutions are comparable to that in pure $BiFeO_3$ at 10 K after the destruction of spiral spin structure under intense magnetic field of ~ 20 T suggests that transition from the modulated spiral spin structure to homogenous spin structure occurs by chemical substitutions also. It also suggests that $M_r$ values close to 0.15 emu/g reported at room temperature in $BiFeO_3$ solid solutions are due to the destruction of the spiral spin structure. This has been confirmed by neutron scattering studies in $Bi(Mn_{0.1}Fe_{0.9})O_3$ and $(Bi_{0.8}Ba_{0.2})$ ( $Fe_{0.8}Ti_{0.2})O_3$ [Sosnowska et al. (2002), Singh et al. (2011)]. Similarly in the $(Bi_{1-x}Ba_x)$ $(Fe_{1-x}$ $Ti_x)O_3$ (BF-xBT) mixed system, remanent magnetization has been reported for x = 0.10 [Singh et al. (2008)] and higher x values with a maximum value of ~ 0.15 emu/g for x = 0.20 [Wang et al. (2005), Wang et al. (2012)]. More recently, in 20% $CaTiO_3$ substituted $BiFeO_3$, remanent magnetization $M_r$ ~ 0.18 emu/g and ~ 0.26 emu/g have been reported at 300 K and 5 K, respectively [Wang et al. (2012)].

In the BF-xBT solid solutions, evidence for linear magnetoelectric coupling at the atomic level has been reported by temperature dependent x-ray diffraction (XRD) and neutron powder diffraction techniques [Singh et al. (2008), Singh et al. (2011)]. However, it is not apriori clear as to why for $x < 0.20$ in the BF-xBT system [Singh et al. (2008)] or in many other $BiFeO_3$ solid solutions, the $M_r$ values are rather low in the range 0.0012 to 0.06 emu/g [Singh Ph.D. thesis (2012), Smolenskii (1965), Paik et al. (2009)] even for lower dilution (10%) of the magnetic sublattice. Is it because the destruction of the spin spiral is not complete? It is of interest to verify in such low $M_r$ systems whether a linear magnetoelectric coupling still exists. The present work seeks to study magnetoelectric coupling in one such system (1-x) $BiFeO_3$-x$Pb(Fe_{1/2}Nb_{1/2})O_3$ (BF-xPFN) with $x = 0.20$ using neutron powder diffraction techniques. The other end member of the BF-xPFN solid solution system, PFN, is also a multiferroic at low temperatures with a $T_N \sim$ 143 K and ferroelectric $T_C \sim 385$ K [Bokov et al. (1962), Smolenskii (1958)]. In the BF-xPFN system with $x = 0.20$, we show that even though the value of $M_r \sim$ 0.0032 emu/g at room temperature is extremely low, it still exhibits magnetoelectric coupling as revealed by a large dielectric anomaly at the magnetic transition temperature $T_N$ and a strong magnetoelastic coupling as indicated by anomalies in the unit cell parameters at $T_N$. These anomalies are furthermore linked with the occurrence of an isostructural phase transition accompanying the magnetic transition at $T_N$ leading to the appearance of significant excess polarization ($\geq 2$ $\mu C/cm^2$) below $T_N$ which scales linearly with the ordered-sublattice magnetization determined from an analysis of the nuclear and magnetic

structures using neutron powder diffraction data. Our work thus confirms that even very weak ferromagnetism with rather small $M_r$ is sufficient to lead to linear magnetoelectric coupling.

## 8.2 Experimental

Polycrystalline samples of BF-0.2PFN were synthesized by solid state reaction route, the details of which have been described in Chapter II. Neutron powder diffraction data as a function of temperature was collected using the high-resolution powder diffractometer SPODI at FRM-II, Germany [Hoelzel et al. (2012)]. The incident neutron wavelength was 1.5483 Å as obtained from Ge 551 reflection of a vertically focused monochromator at 155° takeoff. Approximately 15 g of the sample was contained in a cylindrical niobium (Nb) sample holder with 50 μm wall thickness, 40 mm height and 10 mm diameter for the high temperature measurements in a vacuum furnace. The data was collected with scan step of 0.05° in a 2θ range between 5° and 153°. Rietveld refinements were performed using the FULLPROF software package [Carvajal (2010)]. SARAh software with FULLPROF package was used for symmetry–constrained magnetic structure refinements [Wills (2000)]. The temperature dependent dielectric measurements were carried out in the temperature range 300 K to 723 K at a heating rate of 1 K/min using a Novo Control (Alpha-A) high performance frequency analyzer. The M-H loop and DC magnetization measurements at a magnetic field of 2 kOe were carried out as a function of temperature using a vibrating sample magnetometer (VSM-7410, Lakeshore) at a heating rate of 2 K/min. Differential scanning calorimetric (DSC) measurements were performed by a Mettler DSC827$^e$ at a heating rate of 5 K/min.

## 8.3 Results and discussion

### 8.3.1 Magnetisation and calorimetric studies

The antiferromagnetic transition temperature of $BiFeO_3$ ($T_N$ ~ 643 K) is lowered by PFN substitution. The temperature dependence of the magnetic susceptibility ($\chi$) and ($d\chi/dT$) of BF-0.2PFN is depicted in Fig. 8.1 (a, b). It clearly reveals an anomaly around 566 K characteristic of an antiferromagnetic transition. The antiferromagnetic nature of the transition was confirmed by $1/\chi$ versus T plot also (shown in inset of Fig. 8.1(b)) which gives a negative intercept on the temperature axis on extrapolation of the linear region at high temperatures. Antiferromagnetic transition at $T_N$ ~ 566 K was further confirmed by heat flow measurement which also reveals an anomaly at $T_N$ (see Fig. 8.1 (c)). The antiferromagnetic transition temperature is lowered from 643 K for pure $BiFeO_3$ to 566 K in BF-0.2PFN as a result of the dilution of the magnetic sublattice of $BiFeO_3$ due to 10% $Nb^{5+}$ substitution.

The M-H plot for pure $BiFeO_3$ does not show any hysteresis loop until the magnetic field exceeds ~ 20 T as a result of the destruction of the spin spiral [Wang et al. (2005)]. As a result of 20 % $Pb(Fe_{0.5}Nb_{0.5})O_3$ substitution in $BiFeO_3$ in the BF-0.2PFN composition, one observes a slim M-H loop with $M_r$ ~ 0.0032 emu/g at room temperature as shown in Fig. 8.2. The value of $M_r$ is comparable to the value of $M_r$ ~ 0.0048 emu/g reported by Paik et al. [Paik et al. (2009)] for 10% La substituted BF-0.2PFN but is higher than the value of $M_r$ ~ 0.0012 emu/g

reported by Smolenskii and Yudin [Smolenskii and Yudin (1965)] for the same composition.

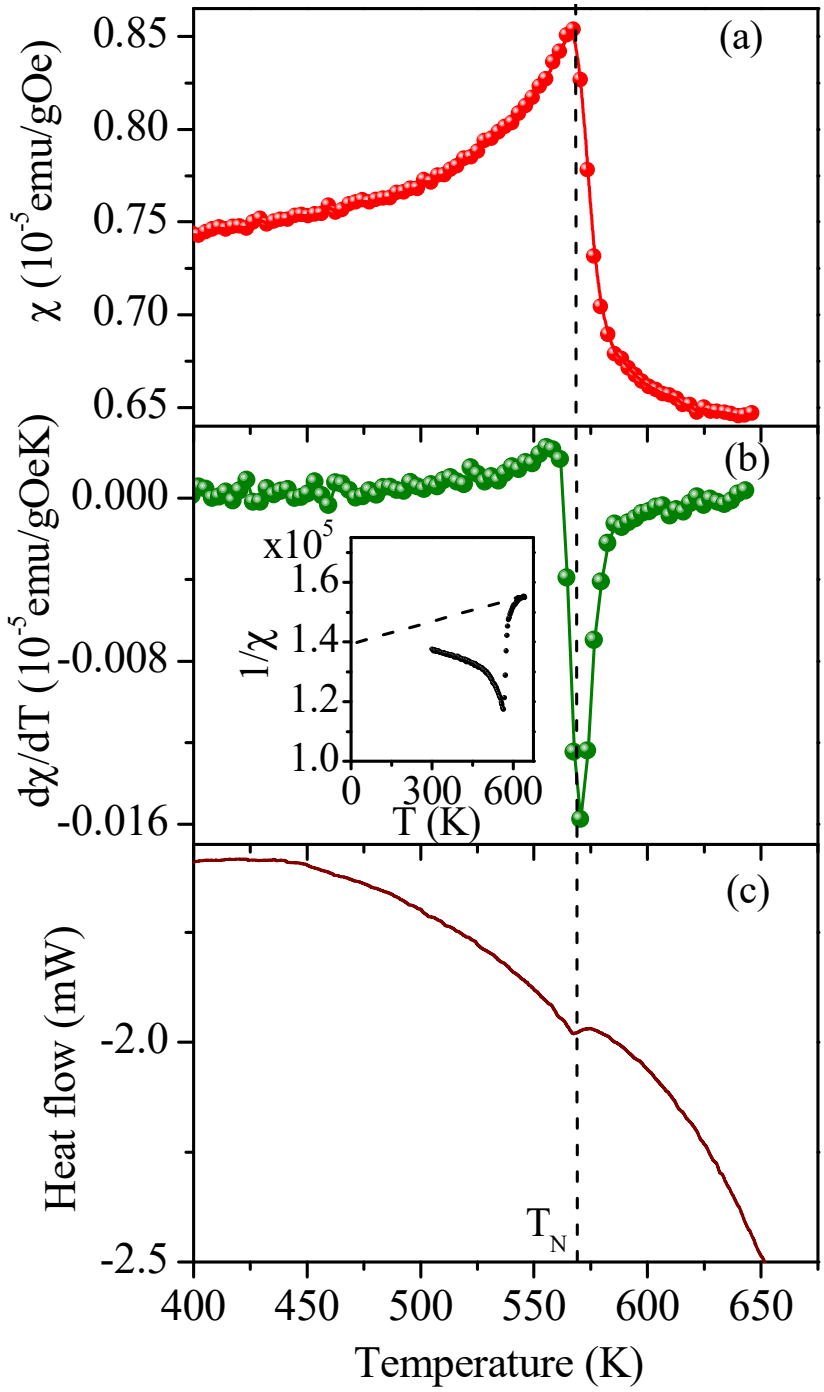


**Fig. 8.1** Variation of the (a) magnetic susceptibility (dots and line) measured at 2 kOe (b) $d\chi/dT$ ($10^{-5}$ emu/gOeK) and (c) heat flow (continuous line) as a function of temperature. Inset of (b) depicts the $1/\chi$ versus T plot.

The weak ferromagnetism of BF-0.2PFN at room temperature is not due to trace amounts of $Fe_2O_3$ present in our samples as the M-H loop disappears just above $T_N$ ~ 566 K as can be seen from the evolution of the loop as a function of temperature shown in Fig. 8.2. Since the loop disappears well below the $T_N$ (~ 955 K) of $Fe_2O_3$, its contribution to the weak ferromagnetism in BF-0.2PFN, if any, is negligibly small [Hill et al. (2008)]. Therefore as a result of 20 % $Pb(Fe_{0.5}Nb_{0.5})O_3$ substitution in $BiFeO_3$, the spin spiral of $BiFeO_3$ is getting suppressed leading to a release of the locked-in weak ferromagnetism on account of spin canting. However, the value of $M_r$ ~ 0.0032 emu/g is rather low as compared to other BF solid solutions [Sosnowska et al. (2002), Wang et al. (2005), Singh et al. (2008), Singh Ph. D. thesis (2012), Wang et al. (2012)].

### 8.3.2 Evidence for Magnetoelastic coupling: x-ray powder diffraction studies

The x-ray powder diffraction patterns recorded above and below $T_N$ ~ 566 K of BF-0.2PFN do not reveal any change of crystal structure. The structure could be refined successfully using the rhombohedral R3c space group both above and below $T_N$ by Rietveld techniques. Fig. 8.3 depicts the fits between the observed and calculated XRD profiles at 300 K (< $T_N$) and 600 K (> $T_N$) obtained by Rietveld refinement. The excellent fits confirm the R3c space group for BF-0.2PFN both below and above $T_N$. This rhombohedral phase remains stable up to

the ferroelectric transition temperature $T_C$ ~ 900 K as discussed in detail in chapter V.

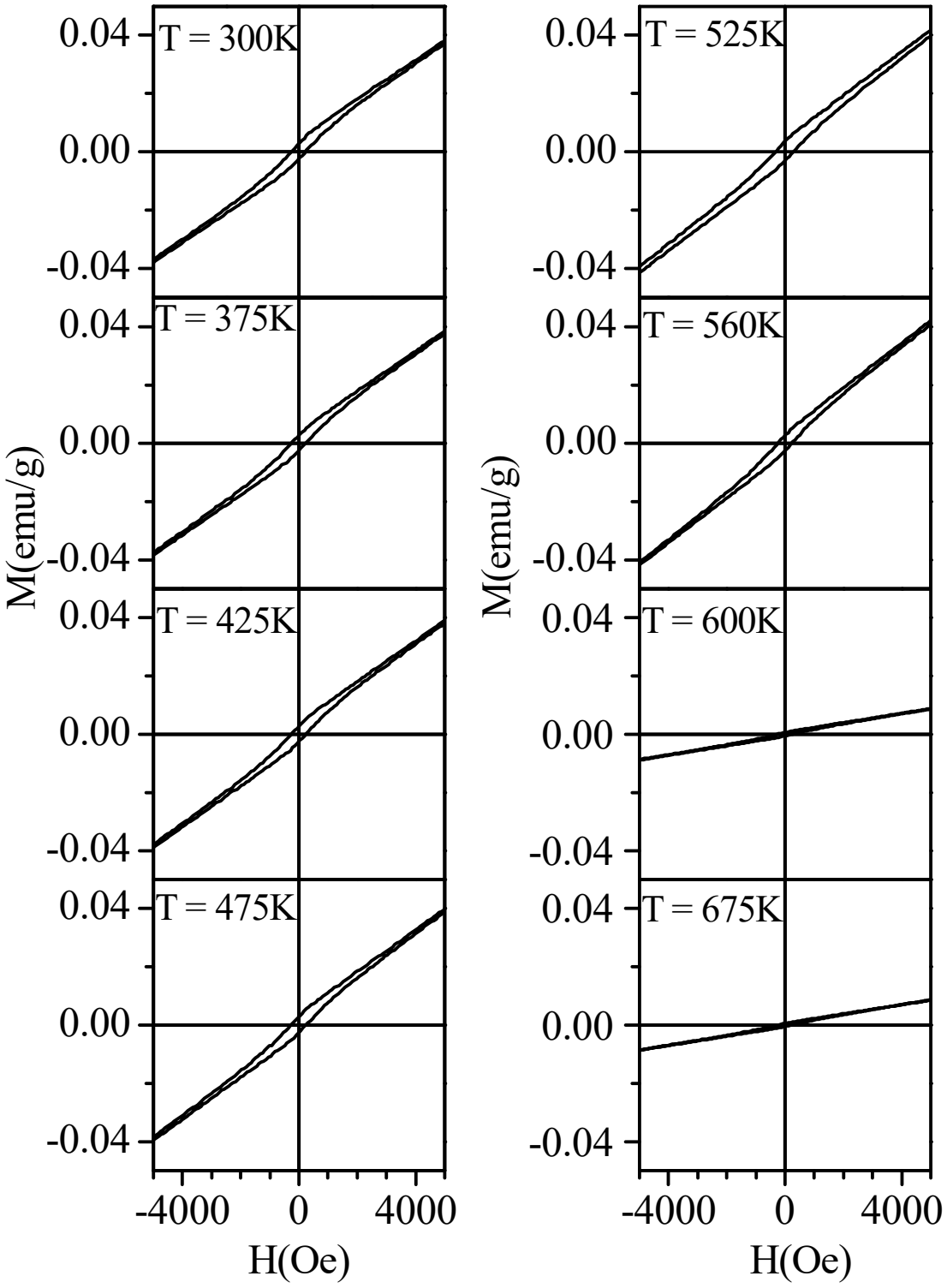


**Fig. 8.2** Magnetisation (M) versus applied magnetic field (H) hysteresis loops of 0.8BF-0.2PFN solid solution at various temperatures above and below the $T_N$.

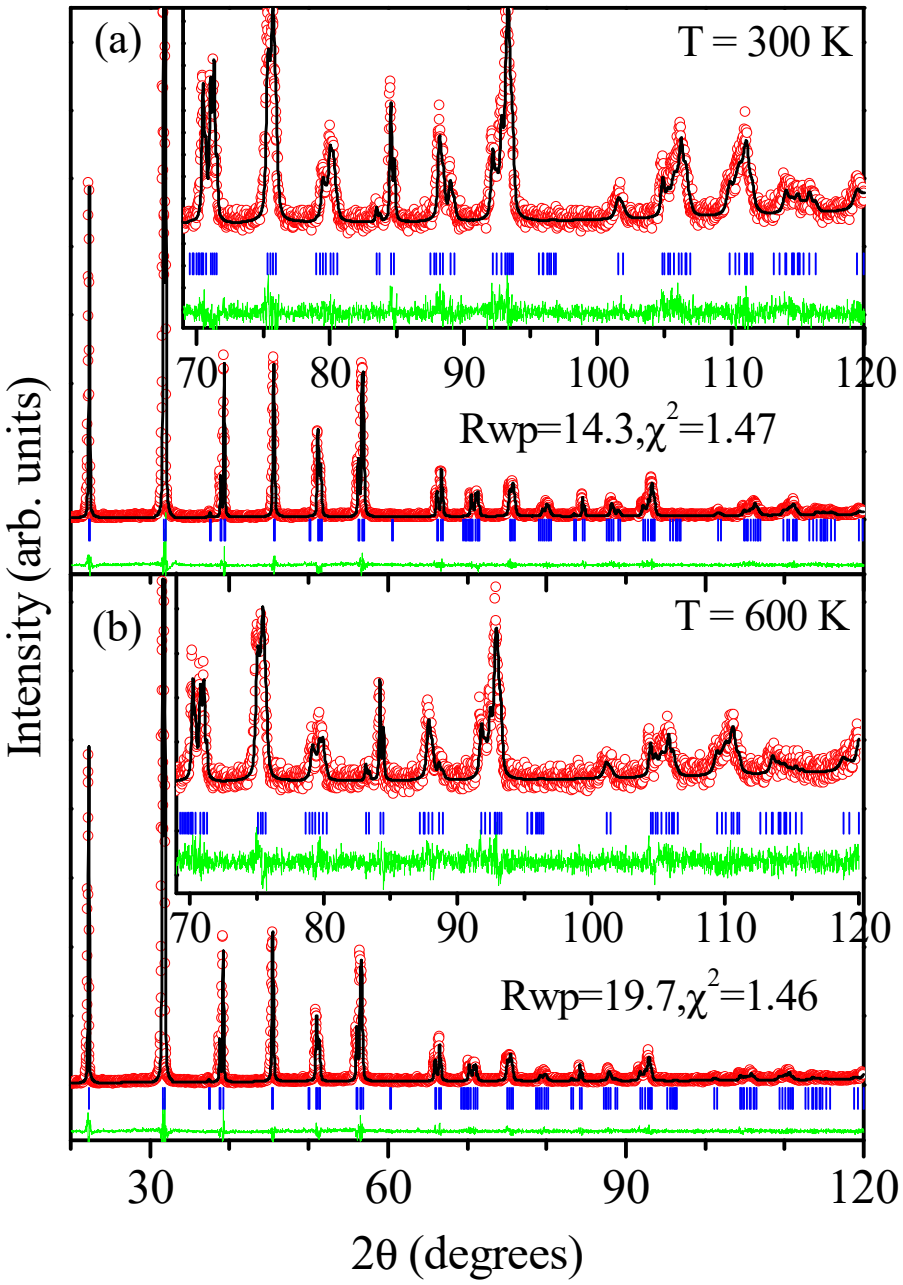


**Fig. 8.3** Observed (dots), calculated (solid line), and difference (bottom line) profiles as obtained from the Rietveld refinement using x-ray diffraction data, at (a) 300 K and (b) 600 K. The tick marks above the difference profiles represent the Bragg peak positions. The insets show the high angle fits at an expanded scale.

While there is no change in the crystal structure across $T_N$, the unit cell volume and rhombohedral distortion angle obtained by Rietveld refinements at various temperatures show pronounced anomalies at $T_N$. This is depicted in Fig. 8.4(a). These anomalies indicate the presence of magnetoelastic coupling in the magnetically ordered phase. The negative slope in the temperature variation of the rhombohedral distortion angle below the $T_N$ is a manifestation of the magnetoelastic coupling.

### 8.3.3 Evidence for magnetoelectric coupling: Dielectric studies

The temperature dependent variation of the dielectric constant of BF-0.2PFN shown in Fig. 8.4(b) reveals a very strong dielectric anomaly at $T_N$ leading to a change in the real part of the dielectric permittivity ($\varepsilon_r^{/}$) by ~ 450 at 1 MHz. It is interesting to note that the value of dielectric constant nearly saturates well below $T_N$ at a value which is significantly higher than the value well above $T_N$. This is a manifestation of the magnetoelectric coupling. At lower frequencies of measurement, we observe still stronger anomalies with flattening of the peak below $T_N$. The strongly frequency dependent part of the anomaly in $\varepsilon_r^{/}$ (T) around $T_N$ is known to be due to electrically heterogeneous microstructure caused by the difference in the conductivities of the grains and grain boundaries in ceramic samples [Singh et al. (2008)]. It is also known that these extrinsic contributions to the dielectric permittivity due to space charges disappear at high frequencies (typically > 100 kHz at high temperature) leaving behind the intrinsic contribution from the ceramic grains only. The strong dielectric anomaly at $T_N$ corresponding to 1 MHz frequency is indicative of intrinsic magnetoelectric coupling free from

space charge contributions coming due to electrically heterogeneous microstructure at lower frequencies.

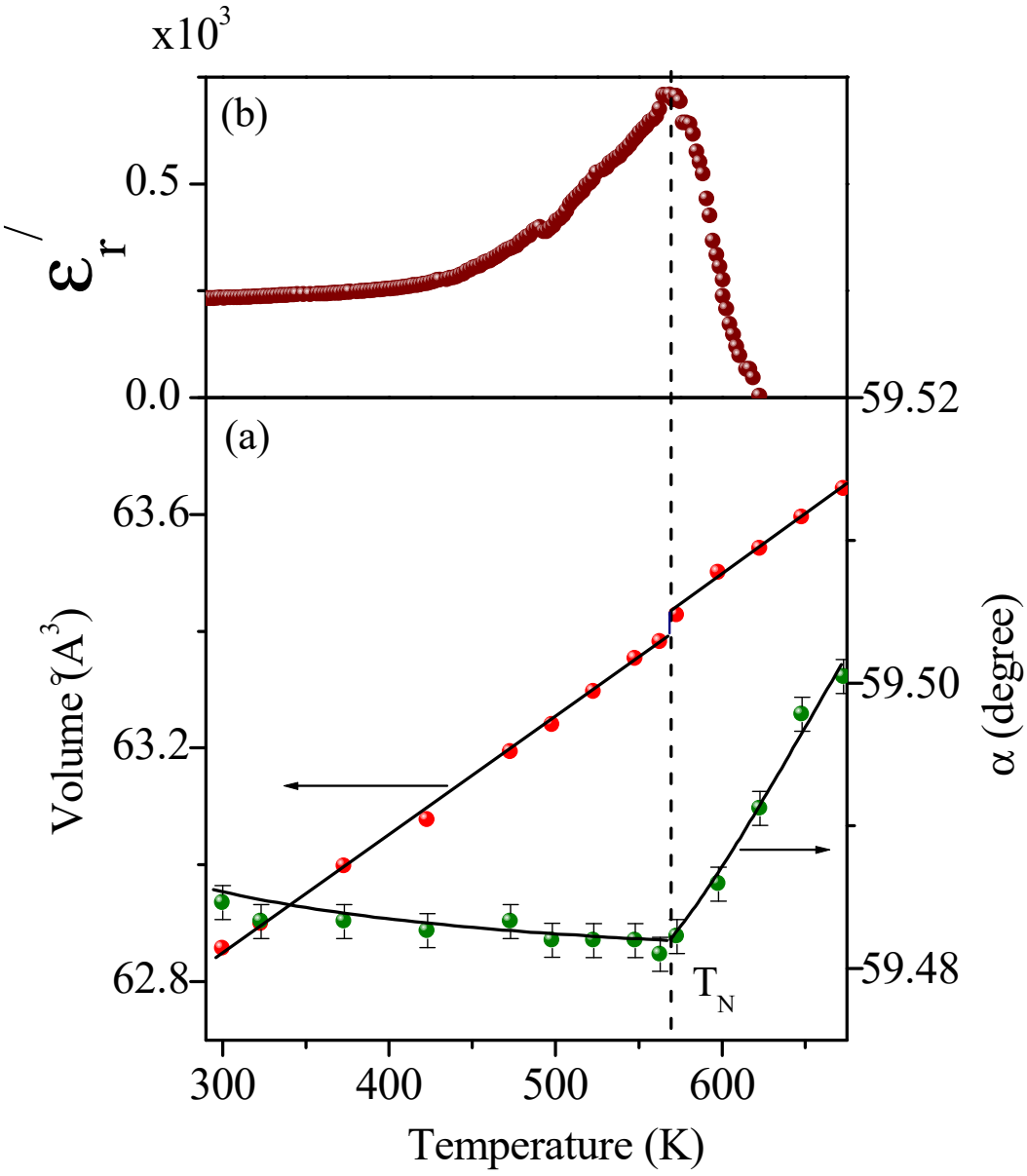


**Fig. 8.4** Variation of the (a) rhombohedral distortion angle $\alpha_{rh}$ and unit cell volume obtained from Rietveld refinements (b) real part of dielectric permittivity ($\varepsilon_r'$) with temperature (T) at 1MHz. The vertical dotted line indicates the magnetic transition temperature ($T_N$).

### 8.3.4 Neutron Powder Diffraction Studies

#### 8.3.4.1Evolution of the neutron powder diffraction profiles across $T_N$

Fig. 8.5 depicts the evolution of the neutron powder diffraction patterns of BF-0.2PFN over 2θ = 15º to 60º range from 300 K to 850 K. All the peaks in this pattern can be indexed with respect to a doubled perovskite cell (~ $2a_p$ x $2a_p$ x $2a_p$). There are two types of reflections in this pattern: those with all even (e) indices (i.e., eee type) from the main perovskite frame work and those with all odd (o) indices (i.e., ooo type) resulting from cell doubling. The presence of superlattice reflections with all odd indices confirms the antiphase tilted oxygen octahedra [Glazer (1972) & (1975)] while the splitting of perovskite peaks confirms rhombohedral symmetry and both confirm the $BiFeO_3$ type structure with R3c space group and $a^- a^- a^-$ tilt system for BF-0.2PFN [Glazer (1972) & (1975)].

However, the superlattice reflections of 'ooo' type with h = k = l, such as the 111 (all Miller indices are with respect to a doubled pseudocubic cell) peak at 2θ ≈ 19.39º, is forbidden by the R3c space group [Glazer (1972) & (1975)]. The intensity of the 111 reflection decreases with increasing temperature and becomes vanishingly small at T ≥ 550 K which is close to $T_N$ ~ 566 K of BF-0.2PFN confirming the magnetic origin of this peak. The small residual intensity of this peak above $T_N$ is probably due to magnetic fluctuations as observed in other $BiFeO_3$ solid solutions also [Singh (2011), Comyn et al. (2009)]. The temperature dependence of the integrated intensity ($I_{111}$) of antiferromagnetic 111 peak, which is proportional to the square of the magnetic order parameters, is shown in Fig. 8.6(a).

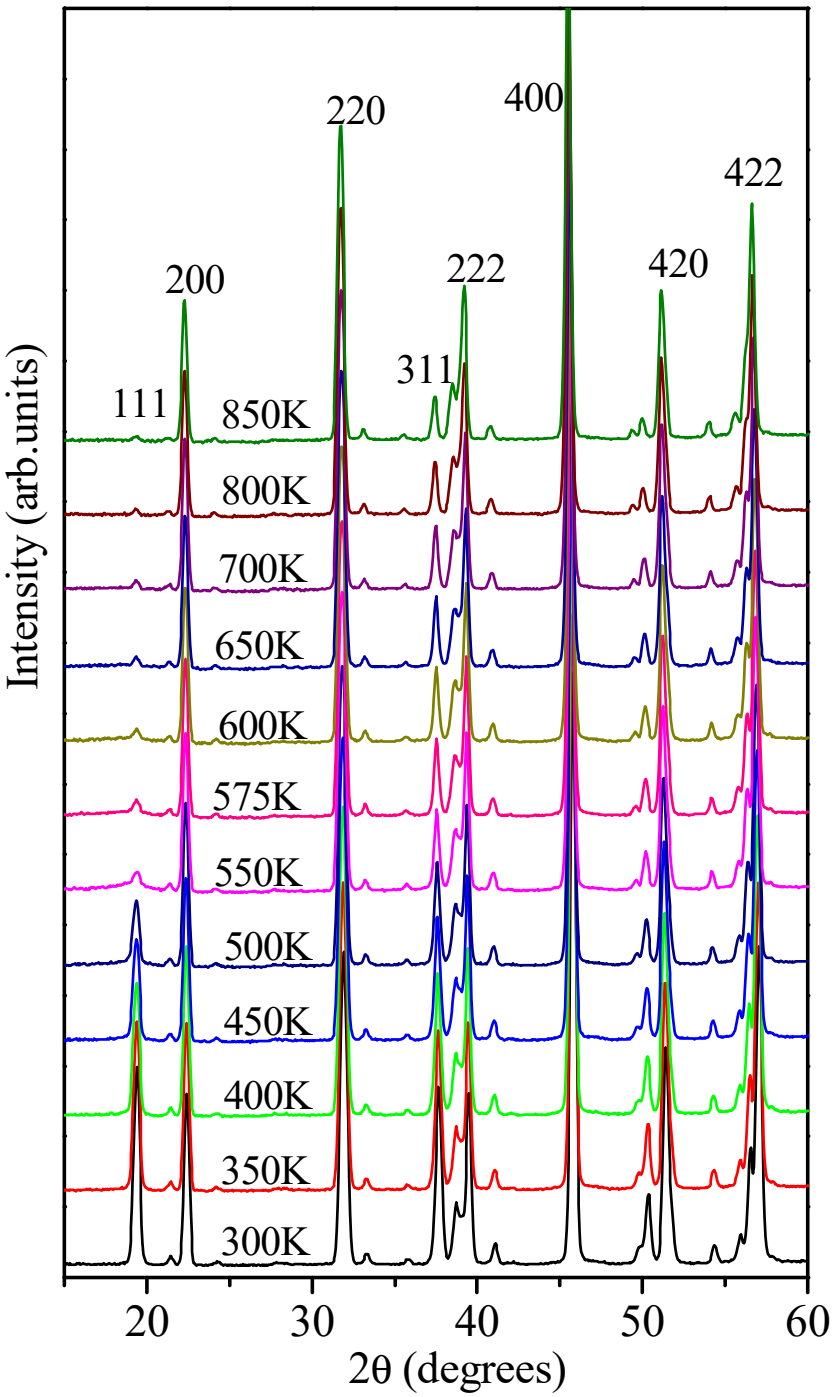


**Fig. 8.5** Evolution of the neutron powder diffraction patterns with temperature in the selected 2θ = 15º to 60º range. The first peak is due to antiferromagnetic ordering. Miller indices are written with respect to doubled pseudocubic cell.

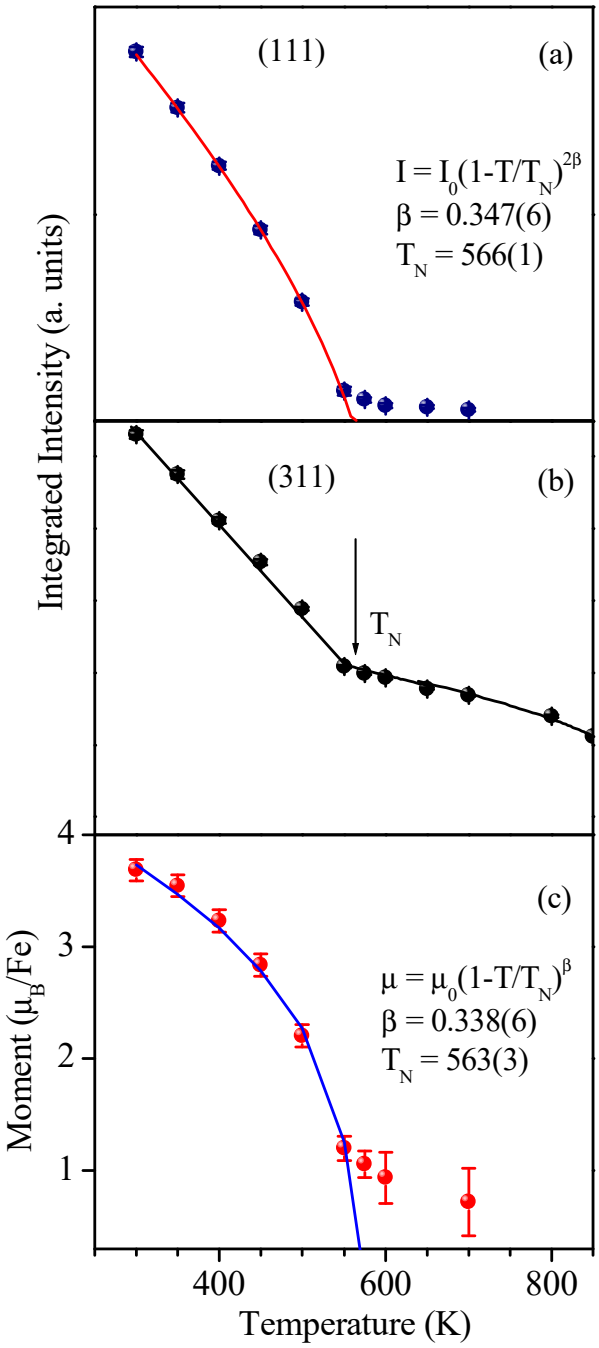


**Fig. 8.6** Temperature dependent variation of (a) integrated intensity of the magnetic peak 111 (Miller indices are with respect to a doubled pseudocubic cell) (filled circles) along with fitted curve (continuous line) corresponding to $I = I_0 (1-T/T_N)^{2\beta}$, (b) the integrated intensity of the 311 (Miller indices are with respect to a doubled pseudocubic cell) peak and (c) ordered magnetic moment (filled circles) obtained from the Rietveld refinements using the neutron diffraction data along with the fitted curve for $\mu = \mu_0 [(T_N-T)/ T_N]^{\beta}$. The arrow in (b) indicates the change in slope of integrated intensity versus temperature plot at $T_N$.

It follows a power law behaviour $(1-T/T_N)^{2\beta}$ characteristics of a second-order like transition. A least square fit to the observed temperature dependence of $I_{111}$ gives $\beta = 0.347(6)$ and $T_N = 566(1)$ K. The value of $T_N$ is in agreement with that obtained by bulk magnetic measurements discussed in the previous section. The value of the critical exponent $\beta$ is comparable to that reported for pure $BiFeO_3$ using neutron scattering and Mössbauer techniques and is in agreement with the predictions for three-dimensional magnetic transitions [Ramazanoglu et al. (2011), Blaauw and Woude (1973)]. The intensity of other superlattice reflections with unequal Miller indices is also affected by magnetic ordering as it decreases drastically above $T_N$. This is illustrated in Fig. 8.6(b) taking 311 superlattice peak as an example which is permitted by the R3c space group for the nuclear structure also due to the antiphase tilting of oxygen octahedra. Accordingly, the intensity of the 311 superlattice reflection is the sum of the contributions from 311 magnetic reflection and 311 nuclear reflection. The sharp change in the curvature of the intensity of the 311 peak versus temperature plot at $T_N \sim 566$ K with drastically reduced intensity above $T_N$ is due to the disappearance of the magnetic contribution to this peak. The residual intensity of the 311 peak above $T_N$ is due to the antiphase tilting of oxygen octahedra.

### 8.3.4.2 Magnetic Structure of the Antiferromagnetic Phase

The room temperature neutron powder diffraction pattern of BF-0.2PFN was analyzed by the Rietveld technique using FULLPROF package [Carvajal (2010)]. The group theoretical representation theory analysis was performed by using SARAh shoftware [Wills (2000)]. The nuclear phase was indexed by using R3c space group while the magnetic phase was indexed by considering the magnetic

phase as a second phase with propagation vector k = (0,0,0) referred to the nuclear phase. The details of the Rietveld refinement of the x-ray and neutron powder diffraction data of BF-0.2PFN at room temperature have already been discussed in chapters III & VII. In this chapter, the temperature dependent x-ray and neutron powder diffraction data were analyzed by using the same procedure.

### 8.3.4.3 Critical exponent at magnetic phase transition

The variation of the refined value of the ordered magnetic moment with temperature is depicted in Fig. 8.6(c). The ordered magnetic moment drops suddenly around 566 K and then steadily goes to vanishingly small values at higher temperatures above 600 K. As in the case of the integrated intensity plot shown in Fig. 8.6(a), the temperature dependence of ordered moment was fitted to a power law $\mu ( T ) = \mu_0 [( T_N - T ) / T_N]^{\beta}$ with $T_N$, $\mu_0$, and $\beta$ as fitting parameters using the data in the temperature range 300 K to 575 K, ignoring the tail behaviour at T > 575 K. The fit is shown as solid line through the data points. The least squares fit gives $\beta$ = 0.338(6) and $T_N$ = 563(3), which are comparable to those obtained from the integrated intensity plot within of course the standard deviations. The value of the critical exponent obtained in our case is very close to 1/3, which differs from $\beta$ = 1/2 value expected on the basis of molecular field theory and Landau theory of second order phase transition. The value of critical exponent found in the present case is comparable to the values obtained for the orthoferrites ($RFeO_3$ where R is the rare earth elements (like La, Pr, Nd etc.)) for which spin- wave theory and Green's- function theory using Callen decoupling also predict an exponent of 1/3 [Eibschütz et al. (1967)].

### 8.3.4.4 Evidence for isostructural phase transition across $T_N$

The enhancement in the dielectric constant around $T_N$ shown in Fig. 8.4(b) clearly suggests modification of the polarization of the lattice in the magnetically ordered phase. Since our samples are not sufficiently insulating, it is not possible to use bulk polarization measurements to confirm the development of excess polarization at $T_N$ due to magnetoelectric coupling. We therefore proceed to seek evidence for the development of excess polarization at $T_N$ by analyzing the atomic positions obtained by Rietveld refinement of the nuclear and magnetic structures of BF-0.2PFN using neutron powder diffraction data. Temperature variation of positional coordinates of all the atoms in the asymmetric unit as obtained by Rietveld analysis of the neutron data is shown in Fig. 8.7. It is evident from this figure that the atomic positions show significant change of slope below $T_N$ with a small discontinuous change for the cations at $T_N$. The shift of atomic positions are consistent with the $\Gamma_1$ mode of the R3c space group at k = (0,0,0) [Singh et al. (2008)] suggesting that the change of atomic positions occurs due to an isostructural phase transition accompanying the magnetic transition at 566 K. It is important to note that in an isostructural phase transition there is no change in the space group and Wyckoff positions across $T_N$.

### 8.3.4.5 Study of the magnetoelectric coupling at the atomic level: Evidence for linear magnetoelectric coupling

It is possible to calculate the ionic polarization under point charge approximation of BF-0.2PFN at various temperatures from the ionic positions shown in Fig. 8.7.

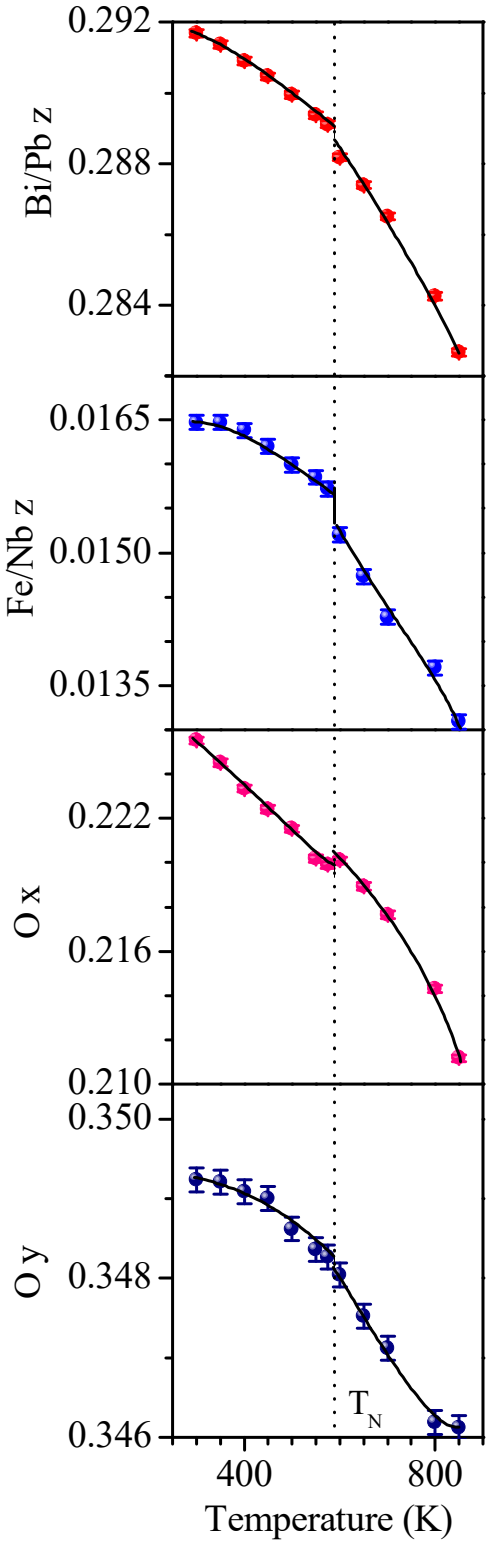


**Fig. 8.7** Temperature dependence of the positional coordinates (a) z of Bi/Pb, (b) z of Fe/Nb, (c) x of O and (d) y of O atoms in the unit cell obtained from the Rietveld refinements using Neutron diffraction data for model III. The dotted vertical line at 566 K indicates the magnetic transition temperature ($T_N$). The standard deviation is less than the size of the dots.

The polarization was calculated by using the formula: $P = (e/V)\sum_k z_k^{/} \Delta(k)$, where $\Delta(k)$ is the displacement of the $k^{th}$ ion from its ideal cubic perovskite position, $z_k^{/}$ is the Born effective charges for the $k^{th}$ ion and V is the volume of the primitive unit cell while the sum runs over all the ions inside the unit cell [Hewat (1973)]. The Born effective charges for $Bi^{3+}$, $Fe^{3+}$ and $O^{2-}$ are taken from the first-principles calculations on multiferroic $BiFeO_3$ while for the $Pb^{2+}$ and $Nb^{5+}$ are taken from the first-principles calculations on $Pb(Fe_{0.5}Nb_{0.5})O_3$[Neaton et al. (2005) and Bhat et al. (2005)]. The polarization of BF-0.2PFN at room temperature, as obtained from Rietveld refined coordinates and Born effective charges, is ~ 86.5(3) $\mu C/cm^2$, which is close to the observed value of ~ 100 $\mu C/cm^2$ for pure $BiFeO_3$ single crystals [Lebeugle et al. (2007A), Lebeugle et al. (2007B)]. The variation of electric polarization P, as obtained using the procedure described above, with temperature is shown in Fig. 8.8(a). From this figure, a significant jump in the ionic polarization by $\Delta P_S$ ~ 1.6(3) $\mu C/cm^2$ at $T_N$ ~ 566 K is evident due to the shift in the positional coordinates of $Bi^{3+}$, $Fe^{3+}$ and $O^{2-}$ at $T_N$. This indicates strong magnetoelectric coupling. The change in polarization ($\Delta P$) at $T_N$ is worth comparing with the spontaneous polarization reported in the multiferroics with improper ferroelectricity to judge its magnitude. The experimentally observed ferroelectric polarizations in $TbMnO_3$, $DyMnO_3$ and $TbMn_2O_5$ are ~ 0.055 $\mu C/cm^2$, 0.135 $\mu C/cm^2$ and 0.04 $\mu C/cm^2$, respectively [Eerenstein et al. (2006), Kimura et al. (2003), Prokhnenko et al.(2007), Kimura et al. (2008) and Wang et al. (2009)]. The change in polarization ($\Delta P$) in BF-0.2PFN at $T_N$ is therefore

atleast one order of magnitude larger than even the total polarization in multiferroics with improper ferroelectricity.

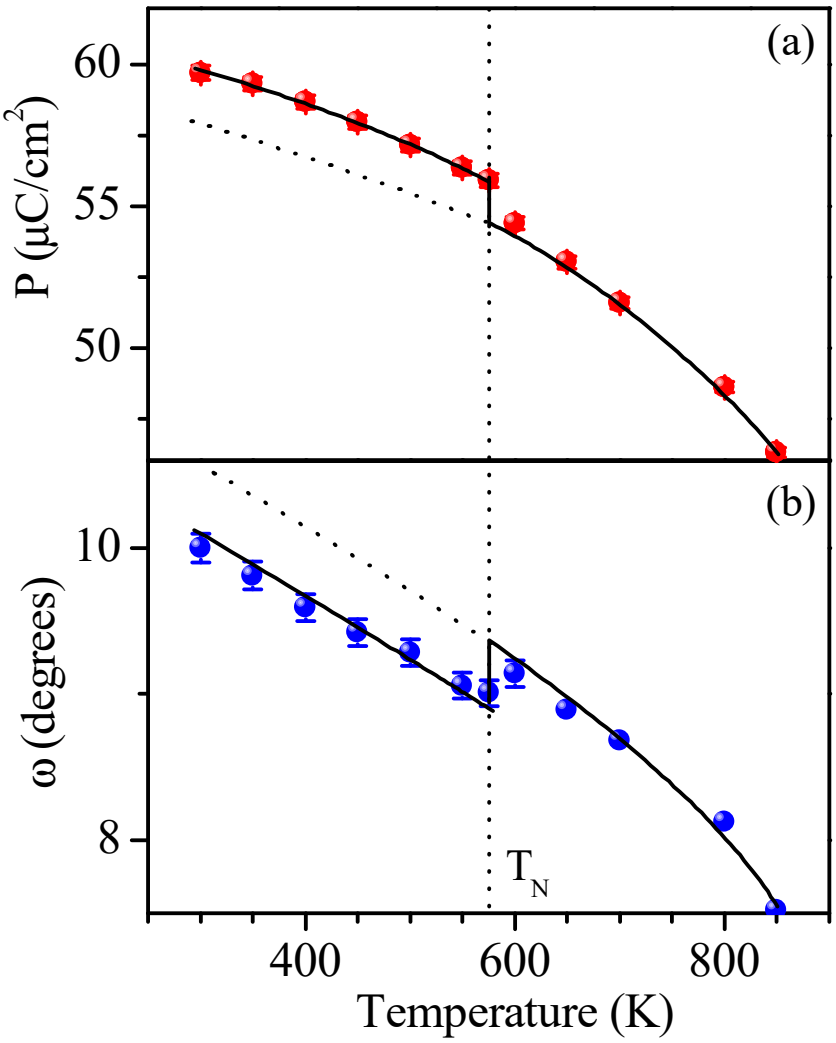


**Fig. 8.8** Temperature dependence of the (a) ionic polarization calculated using positional coordinates of the Bi/Pb z and Fe/Nb z atoms and (b) octahedral tilt angle calculated using positional coordinates of the O x and O y atoms. The dotted curves below $T_N$ show the extrapolated polarization and tilt angle in the magnetically ordered phase below $T_N$. The vertical dotted line shows $T_N$. The standard deviation is less than the size of the dots for ionic polarization and octahedral tilt angle.

It is interesting to mention that not only the polarization changes discontinuously at $T_N$ but the octahedral tilt angle also, as shown in Fig. 8.8(b), which confirms the

first order character of the isostructural phase transition. The octahedral tilt angle (ω) was calculated using the expression $\omega = \tan^{-1} 4\sqrt{3}\ e$, where 'e' is determined from the refined oxygen coordinates [Megaw (1975)]. The variation of the calculated ionic polarization in the magnetically ordered phase with the ordered sublattice magnetization, obtained from the Rietveld refined values of the ordered moments, is plotted in Fig. 8.9. The linear relationship between the calculated ionic polarization and sublattice magnetization confirms the existence of linear magnetoelectric coupling in BF-0.2PFN. It is important to note that the values of P and M used in Fig. 8.9 have been obtained from parameters determined by Rietveld refinement of the nuclear and magnetic structures, respectively. No bulk property measurement technique was used for the determination of P and M shown in Fig. 8.9 and hence our results provide atomic level evidence for linear magnetoelectric coupling

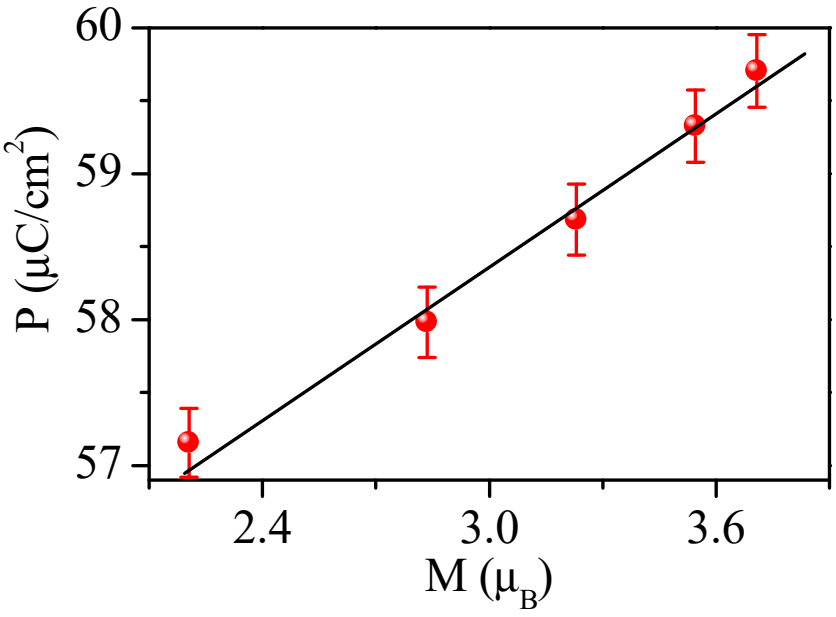


**Fig. 8.9** Variation of the calculated ionic polarizations below T < 566 K with ordered sublattice magnetizations obtained from Rietveld refinement of the nuclear and magnetic structures, respectively. The linear nature of the plot confirms linear magnetoelectric coupling.

## 8.4 Summary and Conclusions

The main conclusions of this chapter may be summarized as under: (i) BF-0.2PFN shows weak ferromagnetism with $M_r$ ~ 0.0032 emu/g at 300 K and an antiferromagnetic transition $T_N$ = 566 K. (ii) Strong anomalies in the dielectric permittivity ($\varepsilon_r'$) are observed at $T_N$ leading to change in $\varepsilon_r'$ by as much as 450 at 1 MHz frequency, at which only the intrinsic contributions to $\varepsilon_r'$ are observed. (iii) There is significant shift in the positions of the ions obtained from the Rietveld refinement of the nuclear and magnetic structures using neutron powder diffraction data below the magnetic transition temperature without affecting the symmetry of the high temperature paramagnetic phase of the BF-0.2PFN due to an isostructural phase transition (IPT). (iv) The ionic polarization and the octahedral tilt angle as obtained from the nuclear structure show significant discontinuous change ($\Delta P_s \simeq 1.6(3)$ μC/cm$^2$ and ($\Delta\omega$ ~ 0.3 degree) confirming first order character of the isostructural phase transition. It also reveals the presence of strong magnetoelectric and magnetoelastic coupling. (v) The ionic part of the ferroelectric polarization as obtained from Rietveld refined coordinates scales linearly with sublattice magnetization, obtained from the refinement of the magnetic structure below $T_N$ providing atomic level evidence for linear magnetoelectric coupling in BF-xPFN inspite of the low value of $M_r$.